Structure
Article

Unraveling the Allosteric Mechanism of Serine Protease Inhibition by an Antibody

Rajkumar Ganesan,[1] Charles Eigenbrot,[1,2] Yan Wu,[2] Wei-Ching Liang,[2] Steven Shia,[1] Michael T. Lipari,[1] and Daniel Kirchhofer[1,*]
[1]Department of Protein Engineering
[2]Department of Antibody Engineering
Genentech, Inc., South San Francisco, CA 94080, USA
*Correspondence: dak@gene.com
DOI 10.1016/j.str.2009.09.014

SUMMARY

Recent structural studies have outlined the mechanism of protease inhibition by active site-directed antibodies. However, the molecular basis of allosteric inhibition by antibodies has been elusive. Here we report the 2.35 Å resolution structure of the trypsin-like serine protease hepatocyte growth factor activator (HGFA) in complex with the allosteric antibody Ab40, a potent inhibitor of HGFA catalytic activity. The antibody binds at the periphery of the substrate binding cleft and imposes a conformational change on the entire 99-loop (chymotrypsinogen numbering). The altered conformation of the 99-loop is incompatible with substrate binding due to the partial collapse of subsite S2 and the reorganization of subsite S4. Remarkably, a single residue deletion of Ab40 abolished inhibition of HGFA activity, commensurate with the reversal of the 99-loop conformation to its "competent" state. The results define an "allosteric switch" mechanism as the basis of protease inhibition by an allosteric antibody.

INTRODUCTION

Allostery, aptly termed the "second secret of life," is an efficient mechanism for the modulation and regulation of protein activity (Fenton, 2008; Monod, 1971). Conformational plasticity is a key intrinsic property that confers on proteins the ability to be allosterically modulated in order to accomplish a variety of cellular functions (Changeux and Edelstein, 2005; del Sol et al., 2009; Krauss, 2003). In fact, all dynamic proteins (monomeric and multimeric) seem to have a potential for allosterism (Gunasekaran et al., 2004). Elucidation of allosteric modulation and its pathways of communication has received considerable attention (Swain and Gierasch, 2006; Yu and Koshland, 2001). A classic example of allostery is observed in hemoglobin (Perutz, 1970), which offered the first mechanistic insights on allosteric regulation. Several X-ray crystallographic studies emerged thereafter describing the conformational changes during allosteric regulation (Changeux and Edelstein, 2005; Di Cera, 2006; Pellicena and Kuriyan, 2006; Xu et al., 1997). Allostery is also a quite common and powerful mechanism to regulate the catalytic activity of proteases (Hauske et al., 2008; Turk, 2006). Examples of allosteric regulators in the serine protease family (Clan PA, Family S1 in MEROPS nomenclature [Rawlings et al., 2008]) are the accessory PDZ domains in the HtrA protease family (Sohn et al., 2007), calcium for many coagulation factors (Bjelke et al., 2008), sodium for thrombin (Huntington, 2008; Wells and Di Cera, 1992), cofactors such as tissue factor for coagulation factor VIIa (Eigenbrot and Kirchhofer, 2002), and N-terminal peptide insertion into the "activation pocket" (Friedrich et al., 2003; Huber and Bode, 1978).

Many proteases have been implicated in human pathological processes (Barrett et al., 1998; Egeblad and Werb, 2002; Hooper, 2002; Luttun et al., 2000). Therefore, regulation of proteolytic activity by allosteric inhibitors might represent a promising alternative approach to active-site inhibitors (Peterson and Golemis, 2004), which often suffer from inadequate specificity, because active-site topologies are generally conserved among members of the same family (Hedstrom, 2002). Unlike active sites, distally located allosteric sites are usually less conserved and can be exploited to achieve specificity (Hauske et al., 2008). Excellent examples of specific and potent allosteric inhibitors have been described for coagulation factor VIIa and caspases (Hardy et al., 2004; Hardy and Wells, 2009).

To exploit allosteric protease inhibition for therapeutic purposes, antibodies may be the inhibitor class of choice, because they have exquisite specificity and excellent pharmacokinetic properties and are successfully used to treat various life-threatening diseases (Adams and Weiner, 2005). In addition, nearly half of the proteases in the human genome are extracellular and theoretically accessible to inhibition by antibodies (Farady et al., 2008; Wu et al., 2007). Recent structural studies on protease inhibition by antibodies have provided the first structural insights into the underlying inhibitory mechanisms. Active site-directed antibodies that sterically block substrate access utilize their complementarity determining region (CDR) loops to embrace critical protease surface loops of the substrate binding cleft and insert one or two CDR heavy chain loops into the cleft to occupy important substrate binding subsites (Farady et al., 2008; Wu et al., 2007). On the other hand, despite structural data on an allosteric antibody, the precise inhibitory mechanism remained elusive (Wu et al., 2007).

To obtain a clear understanding of antibody-mediated allosteric protease inhibition, we used hepatocyte growth factor activator (HGFA) (Kataoka et al., 2003; Miyazawa et al., 1993) as a model system. HGFA is a prototypic extracellular trypsin-like

Table 1. Antibody Binding to HGFA

	HGFA			HGFA-KQLR Complex		
	k_{on} ($\times 10^{-5}$ M^{-1} s^{-1})	k_{off} ($\times 10^{-4}$ s^{-1})	K_D (nM)	k_{on} ($\times 10^{5}$ M^{-1} s^{-1})	k_{off} ($\times 10^{-4}$ s^{-1})	K_D (nM)
Ab39	5.2 ± 0.5	53.0 ± 2.0	10.3 ± 1.3	n.d.	n.d.	n.d.
Ab40	10.8 ± 0.46	1.75 ± 0.08	0.16 ± 0.01	3.2 ± 0.14	4.3 ± 0.13	1.35 ± 0.1
Ab40.ΔTrp[a]	—	—	150 ± 9.1	—	—	161 ± 7.6

Throughout the manuscript, we designated the IgG form of antibody with prefix Ab and the Fab form with prefix Fab. The amino acids of Fab are indicated with a letter-code followed by the residue number, followed by H for heavy chain and L for light chain. n.d., not determined.
[a] The K_D values were determined using steady-state affinity measurements.

serine protease with restricted substrate specificity. Only two macromolecular substrates, pro-hepatocyte growth factor (pro-HGF) (Shimomura et al., 1995) and pro-macrophage stimulating protein (pro-MSP) (Kawaguchi et al., 2009), are known to be processed by HGFA, exemplifying the enzyme's highly restricted substrate specificity. HGFA is inhibited by the Kunitz-type inhibitor HGFA inhibitor 1, which utilizes the N-terminal Kunitz domain 1 (KD1) to inhibit HGFA by a canonical inhibition mechanism (Shia et al., 2005). HGFA effects tissue regeneration and promotes cancer growth via pro-HGF processing and ensuing activation of the HGF/Met signaling pathway (Parr and Jiang, 2001).

Here we describe the generation of a high-affinity anti-HGFA antibody and use enzyme assays and three X-ray structures to show its inhibitory activity is allosteric in nature. Furthermore, the structural results reveal a distinct conformational change transmitted from the antibody epitope to the enzyme substrate binding cleft that can be relieved by a single amino acid deletion in the antibody. In this way, both the origin and the final readout of an allosteric influence are known at the level of single amino acids, along with a complete view of the transmission along all the intervening residues.

RESULTS

Generation of Anti-HGFA Phage Antibody

Ab39 was identified by screening of a synthetic $F(ab')_2$ phage display library (Wu et al., 2007). Ab39 was subsequently affinity-maturated as described in Supplemental Data (available online). The improvement in binding affinity as measured by surface plasmon resonance experiments was 64-fold (Table 1), due to four changes in the sequence of CDR-L3 (Figure 1). The binding specificities of both Ab39 and Ab40 were assessed by using an enzyme-linked immunosorbent assay (ELISA) to measure binding to structurally related proteases, including the closest homologs factor XIIa and urokinase (Miyazawa et al., 1993). The results demonstrated a complete lack of binding to factor XIIa, urokinase, and matriptase, suggesting good specificity (see Figure S1A).

Enzyme Kinetics and Effects of Active-Site Occupancy on Ab40 Binding

Ab40 inhibited the cleavage of pro-HGF into the α/β-heterodimer mediated by HGFA (Figure 2A) with a potency that agreed with its binding affinity (Table 1). The inhibitory effects of Ab39 and Ab40 were also assessed in enzymatic assays using the synthetic *para*-nitroanilide substrate Chromogenix S-2266 (H-D-Val-Leu-Arg-pNA). The enzymatic activity of HGFA was only partially inhibited by Ab40 (Figure 2B), with a maximum inhibition of about 60% under the chosen experimental conditions. Eadie–Hofstee plots demonstrated that the inhibition mechanism was competitive because Ab40 (and Ab39) increased the K_m^{app} but not V_{max}^{app} values (Figure 2C; Figure S1B). In accordance with partial inhibition, the slopes ($-K_m^{app}$) approached a finite limit at high Ab40 concentration. Similar results were obtained with the parental Ab39 (Figure S1B), demonstrating that Ab39 and Ab40 were partial competitive inhibitors of HGFA. To analyze the influence of active site occupancy on the antibody binding, we measured

	CDR-L1											CDR-L2							CDR-L3								
Residue	24	25	26	27	28	29	30	31	32	33	34	50	51	52	53	54	55	56	89	90	91	92	93	94	95	96	97
Ab39	R	A	S	Q	D	V	S	T	A	V	A	S	A	S	F	L	Y	S	Q	Q	S	Y	T	T	P	P	T
Ab40	R	A	S	Q	D	V	S	T	A	V	A	S	A	S	F	L	Y	S	Q	Q	S	N	R	A	P	A	T
Ab40.ΔTrp	R	A	S	Q	D	V	S	T	A	V	A	S	A	S	F	L	Y	S	Q	Q	S	N	R	A	P	A	T
	*	*	*	*	*	*	*	*	*	*	*	*	*	*	*	*	*	*	*	*	*	–	–	–	*	–	*

	CDR-H1						CDR-H2														CDR-H3									
Residue	30	31	32	33	34	35	49	50	51	52	52a	53	54	55	56	57	58	59	60	61	62	63	64	65	94	95	96	97	98	99	100	100a	101	102
Ab39	N	G	T	Y	I	H	G	G	I	Y	P	A	G	G	A	T	Y	Y	A	D	S	V	K	G	K	W	**W**	A	W	P	A	F	D	Y
Ab40	N	G	T	Y	I	H	G	G	I	Y	P	A	G	G	A	T	Y	Y	A	D	S	V	K	G	K	W	**W**	A	W	P	A	F	D	Y
Ab40.ΔTrp	N	G	T	Y	I	H	G	G	I	Y	P	A	G	G	A	T	Y	Y	A	D	S	V	K	G	K	W	–	A	W	P	A	F	D	Y
	*	*	*	*	*	*	*	*	*	*	*	*	*	*	*	*	*	*	*	*	*	*	*	*	*	*	–	*	*	*	*	*	*	*

Figure 1. CDR Sequences of Anti-HGFA Antibodies
The residues are numbered according to the Kabat numbering system (Kabat et al., 1991). The sequence variations between Ab39 and Ab40 are shaded. A single residue deletion (Trp96H) of Fab40 is highlighted in bold.

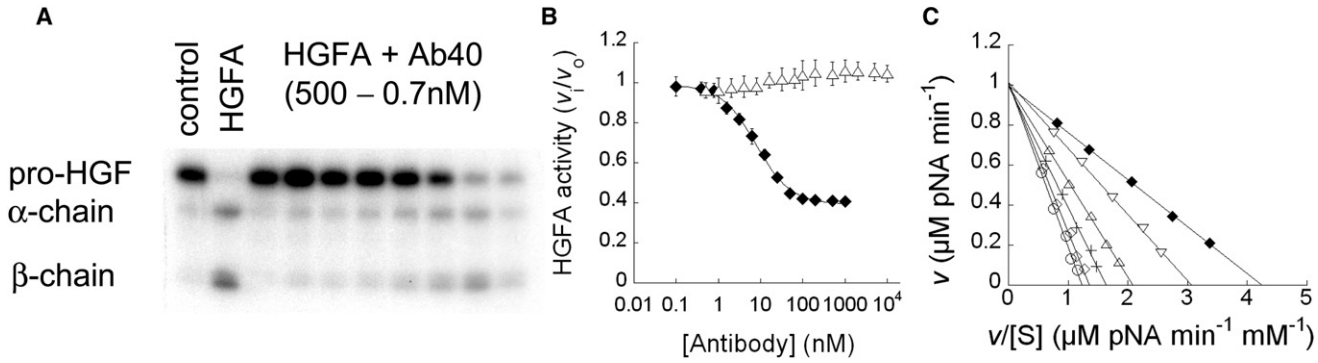

Figure 2. Inhibition of HGFA Enzymatic Activity by Ab40

(A) Cleavage of ^{125}I-pro-HGF by HGFA in presence of 3-fold serial dilutions of Ab40. The cleavage products HGF α and β chain were analyzed by SDS-PAGE (reducing conditions) and subsequent X-ray film exposure.

(B) Partial inhibition of chromogenic substrate, S-2266 hydrolysis (expressed as HGFA fractional activity v_i/v_o) by Ab40 and lack of inhibition by Ab40.ΔTrp. Error bars represent standard deviation (SD).

(C) Eadie-Hofstee plot of HGFA inhibition by Ab40 (1–0.004 μM in 3-fold dilution steps; filled diamonds = "no antibody" control) shows competitive inhibition (V_{max} = 0.99 μM pNA/min and K_m = 0.23 mM for control; V^{app}_{max} = 0.99 μM pNA/min and K^{app}_m = 0.82 mM for 1 μM Ab40).

antibody binding to HGFA in the presence of small-molecule and macromolecular inhibitors. Benzamidine, which only binds in the S1 pocket of trypsin-like serine proteases, did not interfere with binding of Ab40 to HGFA (data not shown). A peptidic inhibitor matching the pro-HGF cleavage sequence coupled to a warhead group (Ac-KQLR-cmk) was used to covalently modify HGFA in the active site, where it occupied the S4-S1 subsites. Surface plasmon resonance studies with HGFA-KQLR complex showed that the irreversibly bound peptidic inhibitor interfered with the binding of Ab40 (Figures 3A and 3B). An 8-fold decrease in affinity of Ab40 binding to HGFA-KQLR complex compared with HGFA was observed (Table 1). The Kunitz domain inhibitor KD1, which interacts with the extended active-site region (Shia et al., 2005), also interferes with Ab40 binding in surface plasmon resonance experiments (Figure 3C). In agreement, a competition ELISA showed moderate inhibition of KD1 binding to HGFA by Ab40 (Figure 3D). In summary, binding of Ab40 to HGFA was influenced by inhibitor occupancy at extended subsites, including S2-S4 but not S1.

Structure of the HGFA/Fab40 Complex Reveals the "Allosteric Switch"

The 2.35 Å resolution structure of the HGFA/Fab40 complex shows that Fab40 uses all six CDR loops to bind to a flat epitope at the periphery of the substrate binding cleft, encompassing the 60-loop and 99-loop (Figures 4A and 4B). The conformation of the catalytic triad (His-57, Asp-102, and Ser-195) has no significant changes compared with other known structures of HGFA (Figure 4B) and the substrate subsites S1-S4 are unoccupied (Figure 5A). The closest atom of Fab40 is > 15 Å from the active site Ser195 residue, indicating an allosteric mode of inhibition. The key feature of the HGFA/Fab40 complex is a large conformational change in the 99-loop (Figure 4B and Figure S2, illustrating the quality of the electron density map). No other significant changes in the HGFA structure are observed suggesting that this is the reason for antibody induced inhibition. The allosteric switch, embodied in the conformation of the 99-loop, is evident from the comparison of the HGFA/Fab40 structure with other structures of HGFA (Shia et al., 2005; Wu et al., 2007), in which the 99-loop is in a "competent" conformation (catalytically active form of HGFA). The Phe97 of the 99-loop in the new conformation ("noncompetent" conformation, catalytically inactive form of HGFA) is buried in a hydrophobic groove formed at the interface of light chain (Tyr49L, Ser50L, and Phe53L) and heavy chain (Trp98H and Pro99H) of Fab40 (Figure 4C). The epitope is centered on Leu-93 of the protruding 99-loop (Figures 5A and 5B), which is sandwiched in a cleft between the CDR loops L3 and H3. The 99-loop and 60-loop are involved in intimate contacts mostly with heavy-chain CDR residues. The heavy and light chains contribute 65% and 35% of buried surface area to the complex, respectively (Figure 5C). The total solvent-accessible surface area of HGFA buried upon Fab40 binding is ~1030 Å^2. Altogether, 17 hydrogen bonds and one electrostatic interaction (Asp241-Lys64H) are formed between HGFA and Fab40 (Table S1). Several hydrophobic residues like Trp95H, Trp96H, Trp98H, and Tyr33H, Tyr52H, Tyr58H bind into small pockets at the back side of the 60- and 99-loops (Figure 4C). The Fab40 epitope on HGFA has significant overlap with a region corresponding to exosite II in thrombin, an electropositive region that interacts with thrombin regulators (Figure 5B). However, unlike exosite II interactions in coagulation proteases, which are primarily electrostatic in nature (Bock et al., 2007), the binding of Fab40 to HGFA involves mainly hydrogen bonding and van der Waals interactions.

Flipping the Allosteric Switch: Engineering Ab40 to Remove the Allosteric Inhibitory Activity

The CDR-H3 loop of Fab40 contains 3 tryptophan residues (Trp95H, Trp96H, and Trp98H) that form the core of the paratope (Figure 5C). Trp96H is central to the observed conformational change in the 99-loop, by docking its large indole side chain in a deep hydrophobic pocket formed by Ala56, Pro90, Tyr88, Val96, Val104, and Ile106 of HGFA (Figure 6A). A small shift in the main-chain as well as the side-chain conformation of Val96 is transmitted through the rest of the 99-loop residues (Val96-Asp100), ultimately leading to > 1 Å root-mean-square deviation (rmsd) shift in C_α (99-loop) (Figures 6C and 6D). To investigate the

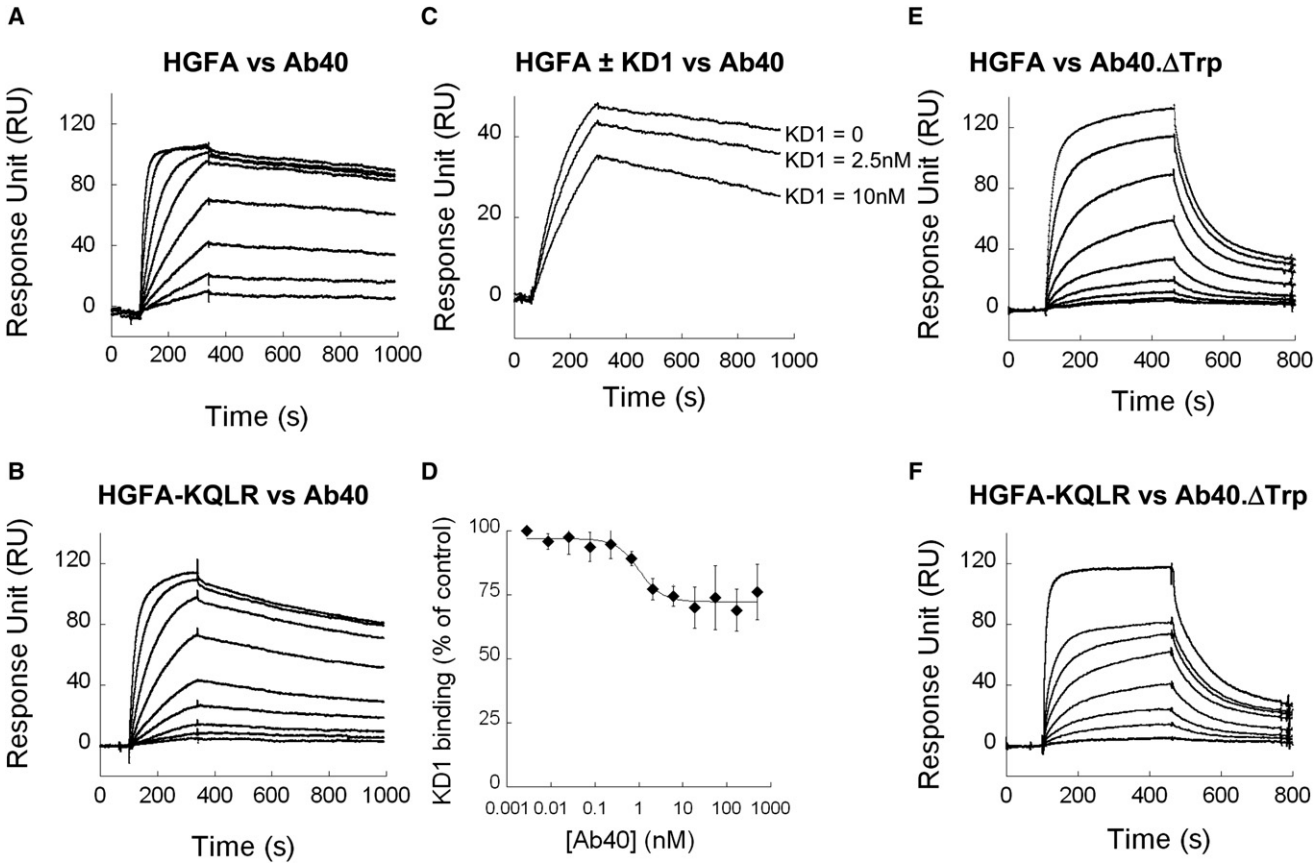

Figure 3. Effects of Active Site Inhibitors on Antibody Binding to HGFA

(A, B, E, F) Surface plasmon resonance (BIAcore) measurements of binding to immobilized antibodies, Ab40 (A, B) or Ab40.ΔTrp (E, F), after coinjection of HGFA (A and E) or HGFA-KQLR (B and F) complex.

(C) Competition binding (BIAcore) of HGFA to immobilized Ab40 in presence of different concentrations of KD1.

(D) Competition binding ELISA measuring binding of HGFA to biotinylated KD1 in the presence of increasing antibody concentrations. Error bars represent SD.

role of Trp96H in the conformational change and the associated allosteric inhibitory activity, we deleted this residue (Fab40.ΔTrp) to shorten the CDR-H3 loop (Figure 1). The complex of HGFA with Fab40.ΔTrp was crystallized as described for the wild-type antibody.

The overall structure of HGFA/Fab40.ΔTrp (2.90 Å) is very similar to that of HGFA/Fab40. The changes are very minimal and confined to residues Ala97H and Trp98H in the CDR-H3 loop (Figures 6E and 6F). The side chain of Tyr33H flips around its χ_1 torsion angle and partly fills the deep hydrophobic pocket that was occupied by Trp96H in the HGFA/Fab40 structure (Figure 6B). The size of this hydrophobic pocket is now reduced due to the movement of residues lining this pocket, principally Ser60, Pro90, and Tyr94 of HGFA. Remarkably the 99-loop reverted to the competent state, as observed in other structures of HGFA (Figures 6E and 6F). Ab40.ΔTrp was no longer an inhibitor of HGFA as determined by enzymatic assays (Figure 2B). It was striking that such a subtle change was enough to remove the inhibitory activity while retaining binding, albeit with much reduced affinity (Table 1). Moreover, unlike Ab40, presence of the KQLR inhibitor in the HGFA active site did not affect Ab40.ΔTrp binding as indicated by the similar K_D values for either HGFA or HGFA-KQLR complex (Figures 3E and 3F). Thus, the data support our hypothesis that the mechanism of allosteric inhibitory activity by Ab40 is primarily driven by a significant change of the 99-loop conformation.

Structural Determinants for the Allosteric Mechanism of Inhibition

The 99-loop of HGFA is a critical substrate specificity determinant by contributing to interactions with substrate residues P2 and P4. Therefore, to obtain a detailed understanding on how the Ab40-induced movement of the 99-loop impacted these substrate subsite interactions, we attempted to determine the structure of the HGFA-KQLR complex. The KQLR sequence corresponds to the P4-P1 residues of the natural HGFA substrate pro-HGF. Unfortunately, these attempts were not successful in producing crystals of sufficient diffraction quality despite several attempts to optimize the crystallization conditions. As an alternative approach, we then focused our attention on solving the structure of HGFA-KQLR in complex Fab40.ΔTrp, which readily crystallized.

The electron density for peptidic inhibitor, Ac-KQLR-cmk was unambiguous in this 2.70 Å resolution structure. The peptidic

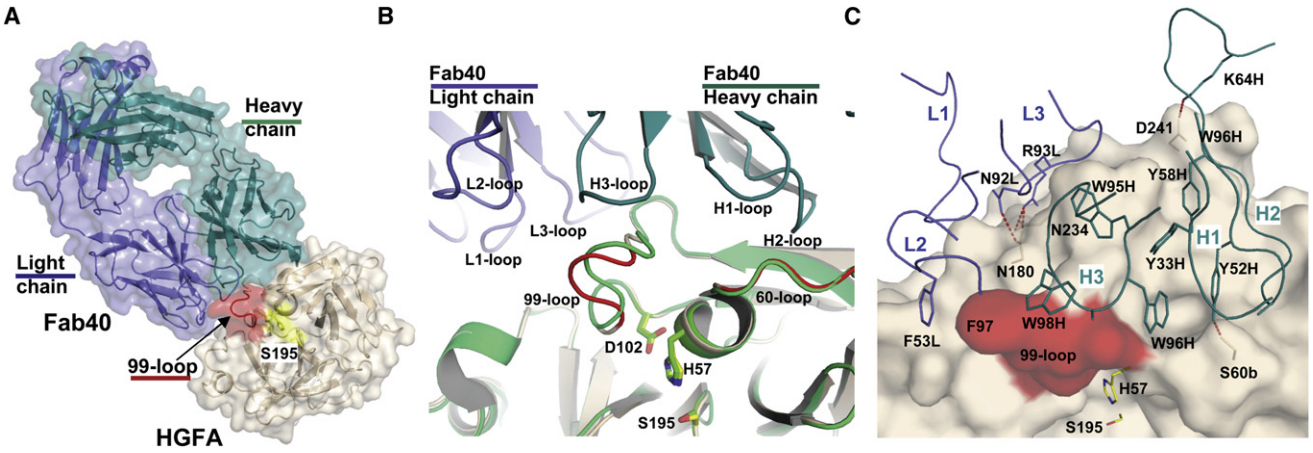

Figure 4. Structure of HGFA/Fab40 Complex

(A) Surface representation with secondary structure highlighted for the complex between HGFA (beige) and Fab40 (light chain in blue, heavy chain in teal). The catalytic triad (His57-Asp102-Ser195) residues are indicated in yellow and the 99-loop is highlighted in red.

(B) Superposition of HGFA/Fab40 (beige) structure with HGFA/Fab75 (Wu et al., 2007) (green) showing no significant changes in the conformation of HGFA except for changes in the 99-loop (red).

(C) A close view of interactions of CDR-loops (L1-3, H1-3) of Fab40 with HGFA (surface representation). Critical residues involved in the interface interactions are highlighted and the 99-loop is indicated in red. Apart from several hydrogen bonds (red dotted line), a single salt bridge between Asp241 of HGFA and Lys64H of Fab40 is observed.

inhibitor aligned in the active site groove in a twisted antiparallel conformation forming the characteristic inter-main-chain hydrogen bonds between P1-Arg and Ser214 and between P3-Gln and Gly216 (Figure S3). The inhibitor was covalently linked to the catalytic Ser195 and His57 and the mode of binding at S4-S1 subsites are very similar to those observed in the complex of KQLR with hepsin, another S1A protease family member (Herter et al., 2005). A salt bridge interaction pairs the P1-Arg of the peptidic inhibitor with Asp189 in the S1 subsite. There appears to be a strong preference for a leucine at the P2 position, because the S2 subsite is a small hydrophobic pocket formed by residues Pro99a, Ser99, Trp215 and His57. The P2-Leu side chain tightly packs against the Pro99a, suggesting that minor changes in the conformation of Pro99a could have a major influence on P2 specificity (Figure 7A). Thus the specificity at the S2 subsite for HGFA appears to be a distinguishing feature, as is the case for many coagulation proteases. Selectivity for the P3 residue is poor in nearly all S1 peptidases because the enzyme–substrate interaction is limited due to solvent exposure of the P3 side chain. The P3-Glu points outward toward the solvent exposed region of the active site. Unlike most S1 peptidases, which possess poor selectivity for a P4 residue, in HGFA a hydrogen bond with Ser99 stabilizes the P4-Lys (Figure 7A). Additionally, hydrophobic stabilization

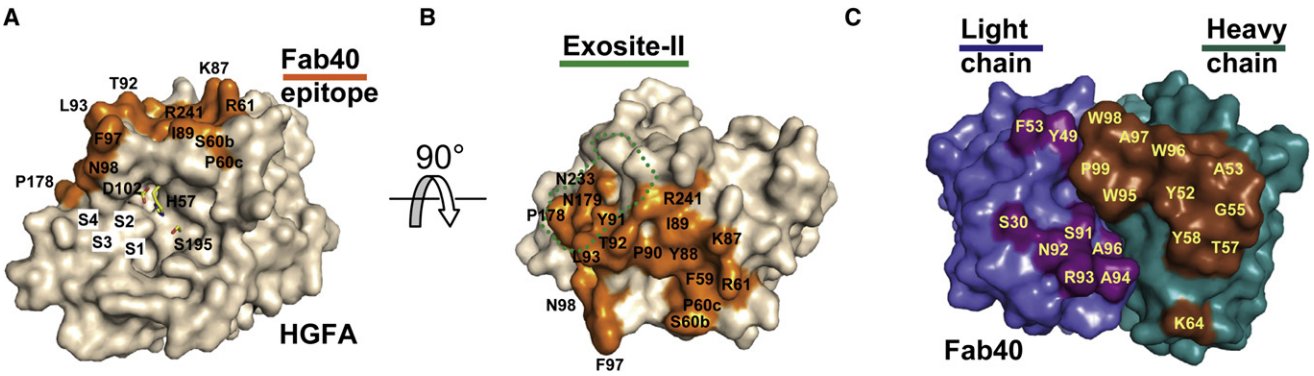

Figure 5. HGFA/Fab40 Epitope and Paratope

HGFA/Fab40 epitope and paratope, with HGFA (beige) and Fab40 (light chain in blue, heavy chain in teal).

(A) Epitope of the Fab40 contact region (orange, 4 Å cutoff) on HGFA (beige).

The catalytic triad and the substrate binding subsites S1-S4 are indicated.

(B) A different view of the Fab40 contact region on HGFA, which has a partial overlap with a region corresponding to exosite-II in thrombin (green).

(C) The HGFA contact region on Fab40 (heavy chain contacts in brown, light chain contacts in purple, 4 Å cutoff). The heavy chain is involved in intimate contacts with HGFA and contributes to two-thirds of the total accessible surface area buried on HGFA upon Fab40 binding.

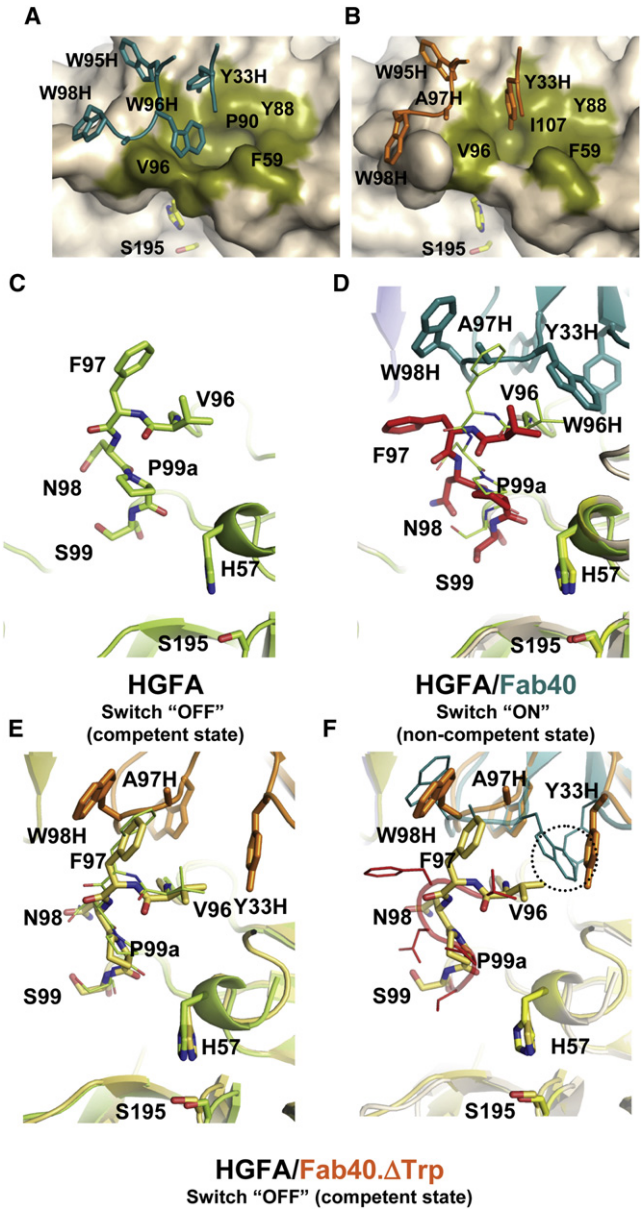

Figure 6. The Three Structural Snapshots of the 99-Loop of HGFA

(A) The allosteric switch in the conformation of the 99-loop leads to the formation of a deep hydrophobic pocket (colored in olive, residues Ala56, Pro90, Tyr88, Val96, Val104, and Ile106 of HGFA) allowing the binding of Trp96H of Fab40.

(B) Size of the hydrophobic pocket (colored in olive) in HGFA/Fab40.ΔTrp is severely restricted due to movement of Val96 and other residues lining this pocket.

(C) The competent state conformation of the 99-loop of HGFA as found in other known structures (Shia et al., 2005; Wu et al., 2007).

(D) Superposition of the 99-loop of HGFA (green) and HGFA/Fab40 (red) complex. Conformation transition of the 99-loop upon Fab40 binding, main chain of the 99-loop residues are shifted by > 1 Å, while the side chain conformations are dislodged by > 2.0 Å. The CDR-H3 loop of Fab40 is highlighted in stick representation (teal).

(E) Superposition of the 99-loop of HGFA/Fab40.ΔTrp with the 99-loop of HGFA. The conformation of the 99-loop (mustard) reverts almost back to the competent state in the Fab40.ΔTrp/HGFA complex structure. The CDR-H3 loop of Fab40. ΔTrp is highlighted in stick representation (orange).

(F) Superposition of the 99-loop of HGFA/Fab40.ΔTrp (mustard) with the 99-loop of HGFA/Fab40 (red), indicating minor changes in CDR-H3 loop upon deletion of Trp96H of Fab40 (dotted circle).

to the side chain of P4-Lys is offered by Trp215 of HGFA. The carbonyl oxygen from the N-terminal acetyl group is interacting with Asp217 of HGFA through a hydrogen bond.

The structure of the protease domain of HGFA in HGFA-KQLR/Fab40.ΔTrp complex is very similar to HGFA/Fab40.ΔTrp complex with rmsd (for all atoms) of 0.39 Å (Figure S4). The conformation of the 99-loop in HGFA-KQLR/Fab40.ΔTrp structure is in the competent state as found in HGFA/Fab40.ΔTrp and other structures of HGFA. Thus, the HGFA-KQLR/Fab40.ΔTrp is a good alternative in the absence of a HGFA-KQLR structure, to define the substrate binding subsites in HGFA. Superposition of HGFA/Fab40 structure with HGFA-KQLR/Fab40.ΔTrp revealed a plausible cause for the allosteric inhibition. The movement of the 99-loop leads to a partial collapse of the subsite S2 and the reorganization of subsite S4, perturbing the interactions with substrate residues P2 and P4. First, the movement of the 99-loop residues Pro99a and Ser99, which are part of the S2 pocket, positions them too close to the P2-Leu (Figure 7B), creating a steric clash. Second, the repositioned hydroxyl side chain of the S4 residue Ser99 can no longer form the hydrogen bond with P4-Lys (Figures 7A and 7B) and is positioned too close to P2-Leu. Furthermore, the movement of the S2 pocket residue Pro99a also plays a key role in defining the allosteric nature of the inhibition of KD1 binding to HGFA by Ab40. Superposition of HGFA/Fab40 and HGFA/KD1 (Shia et al., 2005) complexes showed that there was no overlap between the KD1- and Fab40 epitopes (Figure S5). A model of HGFA/Fab40/KD1 predicts a possibility of Pro99a to sterically clash with Cys38 and Leu39 of KD1 at the S2 subsite.

DISCUSSION

Allosteric regulation of an enzyme, by definition, involves an altered catalytic activity originating from a remote effector interaction site (Tsai et al., 2009). A variety of effectors including binding of small molecules or macromolecules, phosphorylation, etc., result in a signal, which may either activate or inhibit a particular function of the protein (Swain and Gierasch, 2006). Very few such systems are understood beyond knowledge of the effector interaction site and the site of altered activity (del Sol et al., 2009). The exact route by which amino acids transmit the allosteric effect is, in general, very poorly known. Recent studies have provided new insight into the structural basis of protease inhibition by antibodies that target the enzyme active site (Farady et al., 2008; Wu et al., 2007). In contrast, the exact molecular mechanisms by which allosteric antibodies interfere with enzyme catalysis remain elusive. The findings presented herein, derived from comprehensive structural and kinetic studies, now provide a detailed view of how an allosteric antibody inhibits protease catalysis. Enzyme kinetic analysis demonstrates that the phage display-derived Ab40 is a competitive inhibitor of HGFA. Yet, Ab40 did not inhibit by "classical" steric hindrance, because it bound to an epitope distant from the active site, thus defining a competitive inhibition mechanism that is allosteric in nature. Most importantly, the structure of

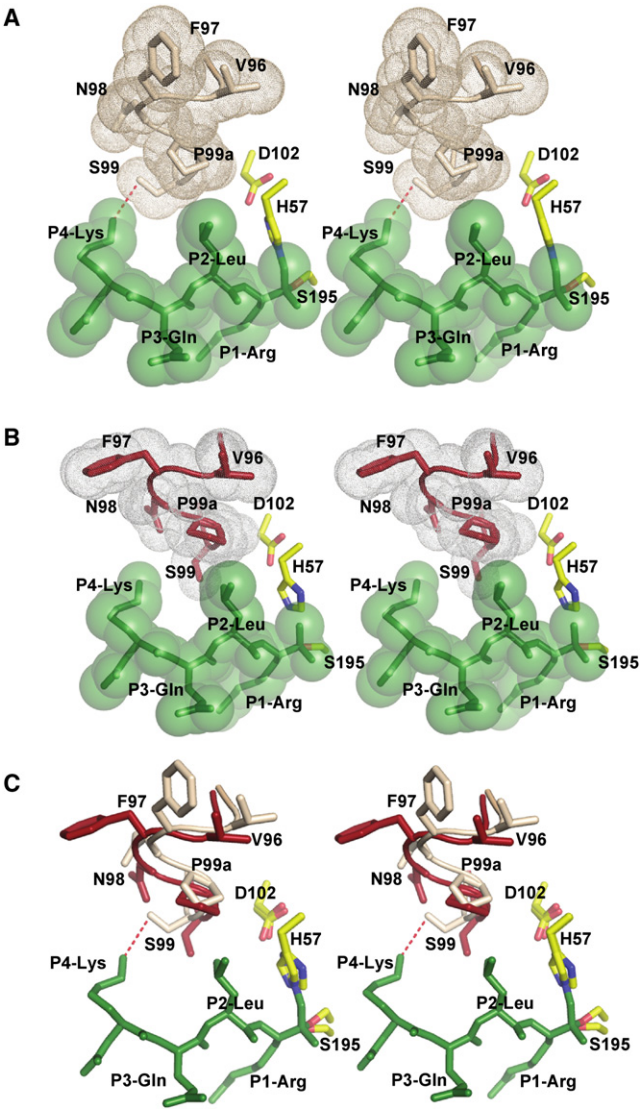

Figure 7. The Allosteric Mechanism

(A) Stereo view of the peptidic inhibitor Ac-KQLR-cmk (sticks embedded in CPK sphere representation in green) is covalently linked to active site Ser195 and His57 of HGFA in the HGFA-KQLR/Fab40.ΔTrp complex. The P2-Leu packs tightly against Pro99a of the 99-loop (sticks embedded in dots representation in beige) and a hydrogen bond with Ser99 stabilizes the P4-Lys.

(B) Stereo view of a model of HGFA-KQLR/Fab40 obtained by from the superposition of HGFA/Fab40 structure with HGFA-KQLR/Fab40.ΔTrp shows that the allosteric inhibition is due to the steric clash between Pro99a and Ser99 with P2-Leu (sticks [red] embedded in dots representation in white).

(C) Stereo view of the superposition of HGFA-KQLR/Fab40.ΔTrp with the model of HGFA-KQLR/Fab40 highlighting the critical conformational changes and disruption of hydrogen bond between Ser99 of HGFA and P4-Lys of the inhibitor.

Fab40/HGFA complex revealed the underlying conformational changes, i.e., the movement of the 99-loop, thereby establishing the structural basis for a functional conduit between epitope and active site.

The observed 99-loop flexibility is unusual in the family of trypsin-like serine proteases, because it is not a part of the so-called activation domain, which comprises several intrinsically mobile surface loops (Huber and Bode, 1978). A known example of conformational flexibility in the 99-loop is observed in the serine protease prostasin (Spraggon et al., 2009).

Ab40 binding was not accompanied by any major structural changes other than the 99-loop movement, strongly indicating that this was the cause for enzyme inhibition. To test this hypothesis, we removed one of the key interactions at the Ab40/HGFA interface, i.e., the hydrophobic contact between Trp96H and Val96 of HGFA. The structure of the generated Trp96H-deletion mutant Ab40.ΔTrp in complex with HGFA showed that the 99-loop had flipped back to the functionally competent state, consistent with assay results showing that the Ab40.ΔTrp/HGFA complex was enzymatically active. Therefore, the 99-loop movement could be considered as an *allosteric switch* regulating enzyme activity: the allosteric switch is turned ON upon Ab40 binding locking the 99-loop in the noncompetent conformation, whereas antibody removal or binding of the Ab40.ΔTrp mutant turns the allosteric switch OFF, allowing the 99-loop to adopt the competent conformation. The question arose as to exactly how the noncompetent 99-loop conformation interferes with the catalytic machinery. That is, which amino acids are changed when Ab40 binds, and why do those changes alter enzyme activity? The 99-loop does not contribute to the formation of the S1 specificity pocket and binding experiments confirmed that S1-P1 interactions were not affected by Ab40 binding. However, the "front" side of the 99-loop in respect to the Ab40 epitope participates in shaping important substrate subsites, and this is the region where obstructions likely arose. The structure of HGFA with the irreversibly bound KQLR peptide provided a plausible answer. The KQLR peptide constitutes the P4-P1 sequence of the natural substrate pro-HGF and also contains the P2-P1 residues, i.e., LR, of the synthetic pNA substrate S-2266 used in our enzyme assays.

Structural analysis showed that the noncompetent conformation of the 99-loop obstructed substrate access to S2 and S4 subsites, due to a steric clash between the P2-Leu and the S2 subsite (Pro99a and Ser99) and the loss of stabilizing interactions between P4-Lys and the S4 subsite. The hydroxyl side chain of Ser99 was found to adopt two different conformations, thus acting as a key specificity determinant at the S2 subsite. This observation is analogous to the conformational changes observed in Tyr99 of coagulation factor IXa (Hopfner et al., 1999). In the competent conformation the hydrophobic S2 pocket is ideally shaped to recognize Leu as a P2 residue, consistent with the presence of P2-Leu in the natural substrates pro-HGF and pro-MSP, as well as the synthetic S-2266 substrate. Therefore, the partial collapse of the S2 subsite by Ab40 binding may have sufficed to cause inhibition of enzyme catalysis toward both macromolecular and synthetic substrates. A caveat associated with this structural interpretation is our use of the HGFA-KQLR/Fab40.ΔTrp structure as a surrogate for that of HGFA-KQLR, which we failed to crystallize. However, the 99-loop in the HGFA-KQLR/Fab40.ΔTrp structure adopts the competent conformation and, therefore, we take this structure as to provide a very good approximation of the S4-S1 interactions with substrate. This view is supported by the observation that the conformation of the KQLR peptide is virtually identical with that in the related KQLR-hepsin complex (Herter et al.,

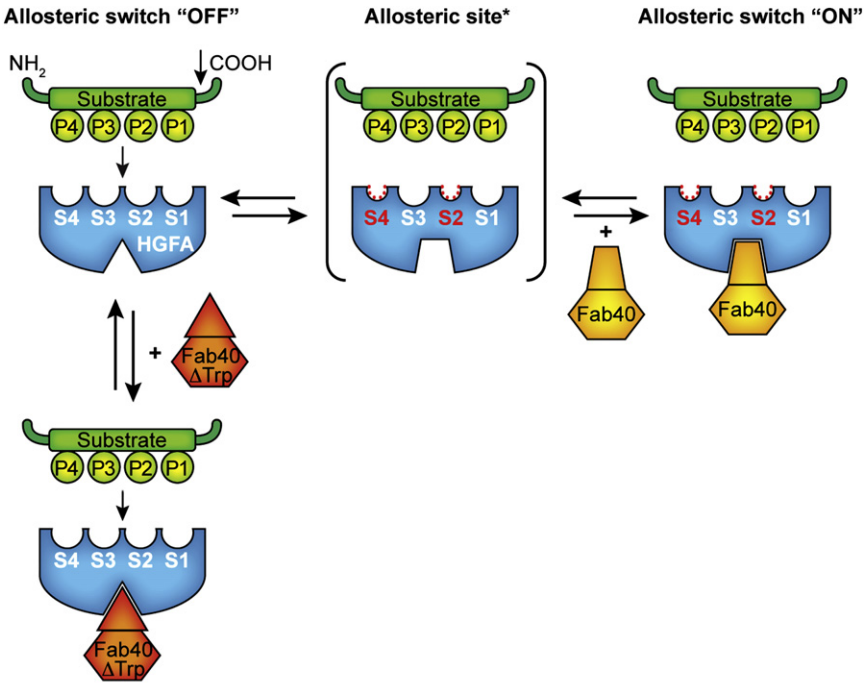

Figure 8. A Cartoon Model Illustrating the Allosteric Mechanism of Inhibition

In the functionally active state, binding subsites are accessible to substrates and the allosteric switch is in the OFF state. Fab40 preferentially samples one of the transiently formed conformations and shifts the equilibrium away from the functionally active state, thus driving the major population of enzyme molecules from the allosteric switch OFF state to the ON state. In contrast, Fab40.ΔTrp, which does not inhibit enzyme activity, might merely bind to the enzyme, without driving a change in state.

2005). We thoroughly evaluated the influence of intermolecular contacts on the interpretation of our results. The catalytic triad (H57-D102-S195) is not involved in crystal contacts in any of the three structures. Additionally, the 99-loop is not involved in crystal contacts in the structure of HGFA/Fab40 or HGFA-KQLR/Fab40.ΔTrp. However, the 99-loop is stabilized by a symmetry-related molecule in the case of HGFA/Fab40.ΔTrp (both molecules in the asymmetric unit). Because the conformation of the 99-loop in HGFA-KQLR/Fab40.ΔTrp is similar as in HGFA/Fab40.ΔTrp, we considered the impact from crystal contacts negligible.

The switch of the 99-loop can be considered as a mobile conduit that connects the inhibitor (i.e., Ab40) binding site with the substrate binding site. Such a view would also provide a suitable framework for understanding the competitive inhibition mode determined in enzymatic assays. Both inhibitor and substrate can apply forces on the 99-loop, albeit from opposite directions, resulting in 99-loop conformations that are suboptimal with either substrate binding (noncompetent state) or inhibitor binding (competent state). Structural models indicate that steric clashes occur in both situations, i.e., between the 99-loop and P2-Leu of substrate in the noncompetent state (Figure 7C) and between the 99-loop and Trp96H, Ala97H, and Trp98H in CDR-H3 of Fab40 in the competent state (Figure S6). Several models of competitive inhibition have been proposed based on classical enzyme kinetics, among them allosteric models, as illustrated by Segel (1993). The elucidated allosteric mechanism is a refinement of the model-5 by Segel, because it provides the structural basis of the molecular linkage between inhibitor binding site and active site. The model in Figure 8 shows the catalytically competent and inhibited states of enzyme in an equilibrium favoring the competent state. In this model, the binding of Ab40 to the transient noncompetent state (allosteric site*, Figure 8) simply shifts the equilibrium away from the functionally active state, thus driving the major population of enzyme molecules from the allosteric switch OFF state to the ON state. The model also accounts for the competitive nature of HGFA inhibition, in that an increase of substrate concentration will shift the equilibrium to the left, i.e., to the competent state of HGFA allowing catalysis to proceed. The mutated Ab40.ΔTrp does not impede catalysis, because it only binds to the competent state in which the allosteric switch is turned OFF. This interpretation is consistent with the generally accepted view of allostery in that effector binding leads to a shift in the ensemble of protein conformations, thus altering the relative populations of particular states. Ab40 binding to HGFA effectively resulted in a shift/redistribution from the competent to a noncompetent state and thus to a functionally impaired enzyme. Extending this view to Ab40.ΔTrp, it can also be regarded as allosteric effector, which imposes only small or negligible effects on the binding site, thereby sampling the competent enzyme conformation.

The allosteric switch is a relatively simple allosteric mechanism. It involves only one mobile surface loop, which directly links the allosteric effector binding site with the active site. It contrasts with other more complex and less understood allosteric mechanisms, such as cofactor-induced enzyme activation (Olsen and Persson, 2008) or PDZ-domain-mediated inhibition/activation of HtrA family members (Sohn et al., 2007), where effector binding is associated with multiple short- and long-range conformational changes. Nevertheless, despite its relative simplicity, it may replicate a naturally occurring allosteric regulation mechanism of HGFA activity by yet unknown effector molecules. In particular, the Ab40 binding site significantly overlaps with the exosite II of thrombin and the corresponding region of coagulation factors IX and X, which are docking sites for various allosteric effectors, including heparin. However, the corresponding region of HGFA appears ill-suited to bind heparin, because the prominent cluster of Arg and Lys residues that mediate exosite-heparin interactions in coagulation factors is minimally represented in HGFA.

Another aspect of our study is the potential usefulness of the anti-HGFA antibody to experimentally address the roles of

HGFA in pathologic pathways. For instance, it was suggested that the ability of HGFA to efficiently process pro-HGF and consequently stimulate the HGF/Met signaling pathway may contribute to cancer growth (Kataoka et al., 2003). Ab40 binds to and blocks mouse HGFA equally well as human HGFA (data not shown), making it an ideal reagent for further investigation of HGFA function in mouse tumor models.

Research on allosteric inhibitors have been actively pursued for kinases (Vajpai et al., 2008) and GPCRs (Raddatz et al., 2007), among others. It is interesting to note that the mechanism of allosteric inhibition by Ab40 is similar to some of the other known allosteric small-molecule inhibitors; in either case, the allosteric inhibitor acts by restricting the conformational flexibility in the enzyme active site (Goodey and Benkovic, 2008; Lee and Craik, 2009). Allosteric anti-protease antibodies may have great therapeutic potential, because they are potent and highly specific and are safeguarded from any inadvertent processing by their target protease. However, their use as therapeutic agents is currently limited to extracellular proteases, whereas intracellular proteases are primarily targeted by orthosteric small-molecule inhibitors. In this respect, our findings may suggest new approaches to identify allosteric "hot spots" that might be amenable to structure-based design of allosterically acting peptidic or small-molecule inhibitor (Hardy and Wells, 2004). Specifically, the herein described interaction of Trp96H with a large hydrophobic pocket (hot spot) is critical in stabilizing the noncompetent 99-loop conformation, yet the existence of this pocket could not have been predicted from other HGFA structures. Thus, large-scale screening of Fab phage display libraries in conjunction with Fab/protease structure determination may identify promising allosteric hot spots. Such an approach should further benefit from the intrinsic property of Fabs to facilitate crystallization of proteins (Tereshko et al., 2008).

EXPERIMENTAL PROCEDURES

Antibody Phage Display

Synthetic antibody libraries displayed bivalent Fab fragments on M13 phage and the diversity was generated by use of oligo-directed mutagenesis in three CDRs of the heavy chain. The details of the Fab libraries were described previously (Lee et al., 2004a, 2004b). Nunc 96-well Maxisorp immunoplates were coated overnight at 4°C with HGFA (10 μg/ml) and then blocked for 1 hr at room temperature with phage blocking buffer PBST (phosphate-buffered saline [PBS], 1% [w/v] bovine serum albumin, 0.05% [v/v] Tween 20). The antibody phage libraries were added to the HGFA-coated plates and incubated overnight at room temperature. The plates were washed with PBT (PBS, 0.05% [v/v] Tween-20) buffer and bound phage were eluted with 50 mM HCl and 500 mM NaCl for 30 min and neutralized with an equal volume of 1 M Tris-HCl (pH 7.5). Recovered phage was amplified in *E. coli* XL-1 blue cells. During subsequent selection rounds, incubation of antibody phage with the antigen-coated plates was reduced to 2–3 hr and the stringency of plate washing was gradually increased.

Antibody Reformatting and Determination of Binding Constants to HGFA

Anti-HGFA Fabs were reformatted into human IgG1 by cloning the V_L and V_H regions of individual clones into LPG3 and LPG4 vector, respectively (Liang et al., 2007). The full-length antibodies were transiently expressed in chinese hamster ovary cells and purified on a protein-A column. To determine binding affinities of the reformatted anti-HGFA antibodies, surface plasmon resonance measurements on a BIAcore-3000 instrument (GE Health Care, NJ) were performed. Rabbit anti-human IgG were chemically immobilized (amine coupling) on CM5 biosensor chips and the anti-HGFA antibodies were captured to give approximately 250 response units (RU). For kinetics measurements, 2-fold serial dilutions of HGFA or active-site-blocked HGFA (0.9 nM to 250 nM) were injected in PBT buffer at 25°C with a flow rate of 30 μl/min. HGFA-KQLR was produced by incubating HGFA with 2-fold molar excess of Ac-KQLR-cmk for 2 hr at room temperature, followed by size exclusion chromatography to remove nonincorporated Ac-KQLR-cmk. Association rates (k_{on}) and dissociation rates (k_{off}) were obtained by using a simple one-to-one Langmuir binding model (BIA-Evaluation) and the equilibrium dissociation constants (K_D) were calculated (k_{off}/k_{on}). Longer injection (5 min) of 2-fold serial dilution of HGFA or HGFA-KQLR (1.5 nM to 3000 nM) over captured antibody (Ab40.ΔTrp) sensor chip was implemented to achieve maximal binding (R_{max}) and reach the steady state. The values of R_{eq} (20%–80% of R_{max}) were calculated and plotted individually against C (concentration of HGFA or HGFA-KQLR) using BIA-Evaluation to determine K_D at the steady-state analysis.

HGFA Purification, Enzyme Kinetic Assays, and Competition ELISA

HGFA (Val373 - Ser655) was produced by use of a baculovirus and insect cell expression system and purified on a Ni-NTA-agarose column, followed by size exclusion chromatography as described previously (Kirchhofer et al., 2003). Pro-HGF activation assays with active-site-titrated HGFA were carried out essentially as described elsewhere (Kirchhofer et al., 2003) using serial dilutions of antibody incubated with 1 nM HGFA and 25 μg/ml ^{125}I-pro-HGF. For chromogenic substrate assays with Chromogenix S-2266 (H-D-Valyl-L-leucyl-L-arginine-*para*-nitroanilide) (Diapharma, Westchester, OH), 5 nM HGFA was incubated for 40 min in 96-well plates with increasing concentrations of antibodies in TNCT buffer (20 mM Tris [pH 8.0], 150 mM NaCl, 5 mM $CaCl_2$, 0.01%-Triton X-100). After addition of S-2266 (0.24 mM ~K_m) the linear rates of the increase in absorbance at 405 nm were measured on a kinetic microplate reader (Spectramax-M5, Molecular devices, Sunnyvale, CA). Enzyme kinetic measurements for Ab39 and Ab40 were carried out with 3 nM HGFA incubated with various antibody concentration (1–0.004 μM in 3-fold dilutions) in TNCT buffer for 40 min. Various concentrations of Chromogenix S-2266 were added and the linear rates of absorbance increase at 405 nm were measured. Eadie-Hofstee plots of the data obtained (v versus v/[S]) were indicative of a competitive inhibition mechanism. Competition ELISA experiments were performed to evaluate effect of Ab40 on KD1 binding to HGFA. A 96-well Maxisorp plate coated with HGFA (1 μg/ml) was incubated with increasing concentrations of Ab40 in PBST buffer for 2 hr, followed by addition of 1 nM biotinylated KD1 for 15 min. Biotinylated KD1 that was bound to HGFA was detected by streptavidin-HRP conjugates.

Crystallography

Fab40 and Fab40.ΔTrp were expressed in *E. coli* and purified by using protein-G sepharose followed by cation exchange chromatography. Complexes between (a) HGFA and Fab40 (b) HGFA and Fab40.ΔTrp or (c) HGFA-KQLR and Fab40.ΔTrp were formed by mixing in a 1:2 molar ratio and purified by size exclusion chromatography (Superdex 200). The complexes were concentrated to ~10 mg/ml in 10 mM HEPES (pH 7.2), 150 mM NaCl. HGFA/Fab40 and HGFA-KQLR/Fab40.ΔTrp complexes yielded crystals under 14% PEG 10,000, 100 mM HEPES (pH 7.2), whereas HGFA/Fab40.ΔTrp yielded crystals under 10% PEG 10,000, 100 mM HEPES (pH 7.5). For X-ray data collection, the crystals were transferred to 14% PEG 10,000, 100 mM HEPES (pH 7.2), 20% glycerol and immersed in liquid nitrogen. X-ray data were collected at 100 K, either at beam line 9-2 at SSRL (HGFA/Fab40) or at ALS beam line 5.0.2 (HGFA/Fab40.ΔTrp and HGFA-KQLR/Fab40.ΔTrp) and reduced using HKL2000 (Otwinowski and Minor, 1997). The structures were solved by molecular replacement using PHASER (McCoy et al., 2005) and refined using CNX (Accelrys) together with elements of the CCP4 suite (CCP4, 1994). Data reduction and model refinement statistics appear in Table 2. We prepared the molecular graphics figures using PyMOL (http://www.pymol.org).

ACCESSION NUMBERS

Coordinates and structure factors for HGFA/Fab40, HGFA/Fab40.ΔTrp and HGFA-KQLR/Fab40.ΔTrp complexes have been deposited at the RCSB Protein Data Bank with access codes 3K2U, 2WUB, and 2WUC, respectively.

Table 2. Data Collection and Refinement

	HGFA/ Fab40	HGFA/ Fab40.ΔTrp	HGFA-KQLR/ Fab40.ΔTrp
Data Collection			
Space group	P1	$P2_1$	$C222_1$
Cell dimensions			
a, b, c (Å)	*a* = 38.94, *b* = 48.93, *c* = 96.03	*a* = 72.36, *b* = 89.53, *c* = 118.47	*a* = 80.36, *b* = 147.89, *c* = 146.37
α, β, γ (°)	α = 98.10, β = 95.01, γ = 103.89	β = 91.08	
Resolution (Å)	50 – 2.35 (2.43-2.35)	50 –2.90 (3.00-2.90)	50 – 2.70 (2.8-2.7)
R_{sym} [a,b]	0.050 (0.198)	0.094 (0.505)	0.143 (0.652)
I/σI [b]	15 (2.9)	14.0 (2.7)	15 (2.9)
Completeness (%) [b]	94.9 (86.9)	98.8 (98.3)	99.4 (97.3)
Redundancy	2.0 (1.9)	3.7 (3.6)	7.3 (7.4)
Refinement			
Resolution (Å)	20 – 2.35	20 – 2.90	20 – 2.70
No. of reflections	25746	32630	23158
Final R [c], R_{free}	0.237, 0.291	0.216, 0.275	0.227, 0.278
No. of atoms			
Protein	5046	9927	5138
Ligand	28	56	68
Water	168	153	133
B-factors (average)			
Protein	65.27	68.92	35.86
Ligand	91.72	138.26	76.06
Water	58.37	39.42	29.65
Rmsd			
Bond lengths (Å)	0.008	0.008	0.007
Bond angles (°)	1.330	1.231	1.420

[a] $R_{sym} = \Sigma||I| - |<I>||/\Sigma|<I>|$, where I is the intensity of a single observation and <I> is the average intensity for symmetry equivalent observations.
[b] In parentheses, for the highest-resolution shell.
[c] $R = \Sigma|Fo-Fc|/\Sigma|Fo|$, where Fo and Fc are observed and calculated structure factor amplitudes, respectively.

SUPPLEMENTAL DATA

Supplemental Data include Supplemental Experimental Procedures, six figures, and one table and can be found with this article online at http://www.cell.com/structure/supplemental/S0969-2126(09)00414-6.

ACKNOWLEDGMENTS

We thank Krista Bowman, Alberto Estevez, and Kyle Mortara for HGFA expression, and Allison Bruce for the graphics. Portions of this research were carried out at the Stanford Synchrotron Radiation Lightsource (SSRL), a national user facility operated by Stanford University on behalf of the U.S. Department of Energy, Office of Basic Energy Sciences. The SSRL Structural Molecular Biology Program is supported by the Department of Energy, Office of Biological and Environmental Research, and by the National Institutes of Health, National Center for Research Resources, Biomedical Technology Program, and the National Institute of General Medical Sciences. The Advanced Light Source is supported by the Director, Office of Science, Office of Basic Energy Sciences, of the U.S. Department of Energy under Contract No. DE-AC02-05CH11231.

Received: May 15, 2009
Revised: September 17, 2009
Accepted: September 18, 2009
Published: December 8, 2009

REFERENCES

Adams, G.P., and Weiner, L.M. (2005). Monoclonal antibody therapy of cancer. Nat. Biotechnol. *23*, 1147–1157.

Barrett, A.J., Rawlings, N.D., and Woessner, J.F. (1998). Handbook of Proteolytic Enzymes (San Diego: Academic Press).

Bjelke, J.R., Olsen, O.H., Fodje, M., Svensson, L.A., Bang, S., Bolt, G., Kragelund, B.B., and Persson, E. (2008). Mechanism of the Ca^{2+}-induced Enhancement of the Intrinsic Factor VIIa Activity. J. Biol. Chem. *283*, 25863–25870.

Bock, P.E., Panizzi, P., and Verhamme, I.M. (2007). Exosites in the substrate specificity of blood coagulation reactions. J. Thromb. Haemost. *5* (*Suppl 1*), 81–94.

CCP4 (Collaborative Computational Project, Number 4). (1994). The CCP4 suite: Programs for protein crystallography. Acta Crystallogr. *D50*, 760–763.

Changeux, J.P., and Edelstein, S.J. (2005). Allosteric mechanisms of signal transduction. Science *308*, 1424–1428.

del Sol, A., Tsai, C.J., Ma, B., and Nussinov, R. (2009). The origin of allosteric functional modulation: multiple pre-existing pathways. Structure *17*, 1042–1050.

Di Cera, E. (2006). A structural perspective on enzymes activated by monovalent cations. J. Biol. Chem. *281*, 1305–1308.

Egeblad, M., and Werb, Z. (2002). New functions for the matrix metalloproteinases in cancer progression. Nat. Rev. Cancer *2*, 161–174.

Eigenbrot, C., and Kirchhofer, D. (2002). New Insight into How Tissue Factor Allosterically Regulates Factor VIIa. Trends Cardiovasc. Med. *12*, 19–26.

Farady, C.J., Egea, P.F., Schneider, E.L., Darragh, M.R., and Craik, C.S. (2008). Structure of an Fab-protease complex reveals a highly specific non-canonical mechanism of inhibition. J. Mol. Biol. *380*, 351–360.

Fenton, A.W. (2008). Allostery: an illustrated definition for the 'second secret of life'. Trends Biochem. Sci. *33*, 420–425.

Friedrich, R., Panizzi, P., Fuentes-Prior, P., Richter, K., Verhamme, I., Anderson, P.J., Kawabata, S.-I., Huber, R., Bode, W., and Bock, P.E. (2003). Staphylocoagulase is a prototype for the mechanism of cofactor-induced zymogen activation. Nature *425*, 535–539.

Goodey, N.M., and Benkovic, S.J. (2008). Allosteric regulation and catalysis emerge via a common route. Nat. Chem. Biol. *4*, 474–482.

Gunasekaran, K., Ma, B., and Nussinov, R. (2004). Is allostery an intrinsic property of all dynamic proteins? Proteins *57*, 433–443.

Hardy, J.A., and Wells, J.A. (2004). Searching for new allosteric sites in enzymes. Curr. Opin. Struct. Biol. *14*, 706–715.

Hardy, J.A., and Wells, J.A. (2009). Dissecting an allosteric switch in caspase-7 using chemical and mutational probes. J. Biol. Chem. *284*, 26063–26069.

Hardy, J.A., Lam, J., Nguyen, J.T., O'Brien, T., and Wells, J.A. (2004). Discovery of an allosteric site in the caspases. Proc. Natl. Acad. Sci. USA *101*, 12461–12466.

Hauske, P., Ottmann, C., Meltzer, M., Ehrmann, M., and Kaiser, M. (2008). Allosteric regulation of proteases. ChemBioChem *9*, 2920–2928.

Hedstrom, L. (2002). Serine protease mechanism and specificity. Chem. Rev. *102*, 4501–4524.

Herter, S., Piper, D.E., Aaron, W., Gabriele, T., Cutler, G., Cao, P., Bhatt, A.S., Choe, Y., Craik, C.S., Walker, N., et al. (2005). Hepatocyte growth factor is a preferred in vitro substrate for human hepsin, a membrane-anchored serine protease implicated in prostate and ovarian cancers. Biochem. J. *390*, 125–136.

Hooper, N.M. (2002). Proteases in Biology and Medicine. In Essays in Biochemistry (London: Portland Press).

Hopfner, K.P., Lang, A., Karcher, A., Sichler, K., Kopetzki, E., Brandstetter, H., Huber, R., Bode, W., and Engh, R.A. (1999). Coagulation factor IXa: the relaxed conformation of Tyr99 blocks substrate binding. Structure *7*, 989–996.

Huber, R., and Bode, W. (1978). Structural basis of the activation and action of trypsin. Acc. Chem. Res. *11*, 114–122.

Huntington, J.A. (2008). How Na+ activates thrombin–a review of the functional and structural data. Biol. Chem. *389*, 1025–1035.

Kabat, E.A., Wu, T.T., Perry, H.M., Gottesman, K.S., and Foeller, C. (1991). Sequences of proteins of immunological interest, Fifth Edition (Bethesda, Maryland: National Institutes of Health).

Kataoka, H., Miyata, S., Uchinokura, S., and Itoh, H. (2003). Roles of hepatocyte growth factor (HGF) activator and HGF activator inhibitor in the pericellular activation of HGF/scatter factor. Cancer Metastasis Rev. *22*, 223–236.

Kawaguchi, M., Orikawa, H., Baba, T., Fukushima, T., and Kataoka, H. (2009). Hepatocyte growth factor activator is a serum activator of single-chain precursor macrophage-stimulating protein. FEBS J. *276*, 3481–3490.

Kirchhofer, D., Peek, M., Li, W., Stamos, J., Eigenbrot, C., Kadkhodayan, S., Elliott, J.M., Corpuz, R.T., Lazarus, R.A., and Moran, P. (2003). Tissue expression, protease specificity, and Kunitz domain functions of hepatocyte growth factor activator inhibitor-1B (HAI-1B), a new splice variant of HAI-1. J. Biol. Chem. *278*, 36341–36349.

Krauss, G. (2003). Biochemistry of Signal Transduction and Regulation (New York: Wiley and Sons), pp. 89–114.

Lee, G.M., and Craik, C.S. (2009). Trapping moving targets with small molecules. Science *324*, 213–215.

Lee, C.V., Liang, W.C., Dennis, M.S., Eigenbrot, C., Sidhu, S.S., and Fuh, G. (2004a). High-affinity human antibodies from phage-displayed synthetic Fab libraries with a single framework scaffold. J. Mol. Biol. *340*, 1073–1093.

Lee, C.V., Sidhu, S.S., and Fuh, G. (2004b). Bivalent antibody phage display mimics natural immunoglobulin. J. Immunol. Methods *284*, 119–132.

Liang, W.C., Dennis, M.S., Stawicki, S., Chanthery, Y., Pan, Q., Chen, Y., Eigenbrot, C., Yin, J., Koch, A.W., Wu, X., et al. (2007). Function blocking antibodies to neuropilin-1 generated from a designed human synthetic antibody phage library. J. Mol. Biol. *366*, 815–829.

Luttun, A., Dewerchin, M., Collen, D., and Carmeliet, P. (2000). The role of proteinases in angiogenesis, heart development, restenosis, atherosclerosis, myocardial ischemia, and stroke: insights from genetic studies. Curr. Atheroscler. Rep. *2*, 407–416.

McCoy, A.J., Grosse-Kunstleve, R.W., Storoni, L.C., and Read, R.J. (2005). Likelihood-enhanced fast translation functions. Acta Crystallogr. D Biol. Crystallogr. *61*, 458–464.

Miyazawa, K., Shimomura, T., Kitamura, A., Kondo, J., Morimoto, Y., and Kitamura, N. (1993). Molecular cloning and sequence analysis of the cDNA for a human serine protease reponsible for activation of hepatocyte growth factor. Structural similarity of the protease precursor to blood coagulation factor XII. J. Biol. Chem. *268*, 10024–10028.

Monod, J. (1971). Chance and Necessity: Essay on the Natural Philosophy of Modern Biology (New York: Knopf).

Olsen, O.H., and Persson, E. (2008). Cofactor-induced and mutational activity enhancement of coagulation factor VIIa. Cell. Mol. Life Sci. *65*, 953–963.

Otwinowski, Z., and Minor, W. (1997). Processing of X-ray diffraction data collected in oscillation mode. In: Macromolecular Crystallography Part A. Methods Enzymol. *276*, 307–326.

Parr, C., and Jiang, W.G. (2001). Expression of hepatocyte growth factor/scatter factor, its activator, inhibitors and the c-Met receptor in human cancer cells. Int. J. Oncol. *19*, 857–863.

Pellicena, P., and Kuriyan, J. (2006). Protein-protein interactions in the allosteric regulation of protein kinases. Curr. Opin. Struct. Biol. *16*, 702–709.

Perutz, M.F. (1970). Stereochemistry of cooperative effects in haemoglobin. Nature *228*, 726–739.

Peterson, J.R., and Golemis, E.A. (2004). Autoinhibited proteins as promising drug targets. J. Cell. Biochem. *93*, 68–73.

Raddatz, R., Schaffhauser, H., and Marino, M.J. (2007). Allosteric approaches to the targeting of G-protein-coupled receptors for novel drug discovery: a critical assessment. Biochem. Pharmacol. *74*, 383–391.

Rawlings, N.D., Morton, F.R., Kok, C.Y., Kong, J., and Barrett, A.J. (2008). MEROPS: the peptidase database. Nucleic Acids Res. *36*, D320–D325.

Segel, I. (1993). Enzyme Kinetics: Behavior and Analysis of Rapid Equilibrium and Steady-State Enzyme Systems (New York: Wiley), pp. 161–226.

Shia, S., Stamos, J., Kirchhofer, D., Fan, B., Wu, J., Corpuz, R.T., Santell, L., Lazarus, R.A., and Eigenbrot, C. (2005). Conformational lability in serine protease active sites: structures of hepatocyte growth factor activator (HGFA) alone and with the inhibitory domain from HGFA inhibitor-1B. J. Mol. Biol. *346*, 1335–1349.

Shimomura, T., Miyazawa, K., Komiyama, Y., Hiraoka, H., Naka, D., Morimoto, Y., and Kitamura, N. (1995). Activation of hepatocyte growth factor by two homologous proteases, blood-coagulation factor XIIa and hepatocyte growth factor activator. Eur. J. Biochem. *229*, 257–261.

Sohn, J., Grant, R.A., and Sauer, R.T. (2007). Allosteric Activation of DegS, a Stress Sensor PDZ Protease. Cell *131*, 572–583.

Spraggon, G., Hornsby, M., Shipway, A., Tully, D.C., Bursulaya, B., Danahay, H., Harris, J.L., and Lesley, S.A. (2009). Active site conformational changes of prostasin provide a new mechanism of protease regulation by divalent cations. Protein Sci. *18*, 1081–1094.

Swain, J.F., and Gierasch, L.M. (2006). The changing landscape of protein allostery. Curr. Opin. Struct. Biol. *16*, 102–108.

Tereshko, V., Uysal, S., Koide, A., Margalef, K., Koide, S., and Kossiakoff, A.A. (2008). Toward chaperone-assisted crystallography: protein engineering enhancement of crystal packing and X-ray phasing capabilities of a camelid single-domain antibody (VHH) scaffold. Protein Sci. *17*, 1175–1187.

Tsai, C.J., Del Sol, A., and Nussinov, R. (2009). Protein allostery, signal transmission and dynamics: a classification scheme of allosteric mechanisms. Mol. Biosyst. *5*, 207–216.

Turk, B. (2006). Targeting proteases: successes, failures and future prospects. Nat. Rev. Drug Discov. *5*, 785–799.

Vajpai, N., Strauss, A., Fendrich, G., Cowan-Jacob, S.W., Manley, P.W., Grzesiek, S., and Jahnke, W. (2008). Solution conformations and dynamics of ABL kinase-inhibitor complexes determined by NMR substantiate the different binding modes of imatinib/nilotinib and dasatinib. J. Biol. Chem. *283*, 18292–18302.

Wells, C.M., and Di Cera, E. (1992). Thrombin is a Na(+)-activated enzyme. Biochemistry *31*, 11721–11730.

Wu, Y., Eigenbrot, C., Liang, W.-C., Stawicki, S., Shia, S., Fan, B., Ganesan, R., Lipari, M.T., and Kirchhofer, D. (2007). Structural insight into distinct mechanisms of protease inhibition by antibodies. Proc. Natl. Acad. Sci. USA *104*, 19784–19789.

Xu, Z., Horwich, A.L., and Sigler, P.B. (1997). The crystal structure of the asymmetric GroEL-GroES-(ADP)7 chaperonin complex. Nature *388*, 741–750.

Yu, E.W., and Koshland, D.E., Jr. (2001). Propagating conformational changes over long (and short) distances in proteins. Proc. Natl. Acad. Sci. USA *98*, 9517–9520.

